1990

Persistence of Residual Currents in the James River Estuary and its Implication to Mass Transport

Albert Y. Kuo

John M. Hamrick

Gamble M. Sisson

Persistence of Residual Currents in the James River Estuary and its Implication to Mass Transport

Albert Y. Kuo, John M. Hamrick, and Gamble M. Sisson

Virginia Institute of Marine Science
College of William and Mary
Gloucester Point, VA 23062

ABSTRACT

The distribution and persistence of Eulerian and Lagrangian residual velocity in a cross sectional transect of the James River estuary, Virginia are analyzed. The Eulerian residual velocity has the characteristic two-layered estuarine circulation in the northern half of the transect, however, the net flow is directed downriver at all depths in the shallower southern half of the transect. In the deep channel, the two-layered Eulerian residual circulation is highly persistent over the six month study duration, with disruptions occurring less than 10% of the time when meteorological forcings are intense. No spring-neap tidal cycle variation is apparent. The magnitude of the long-term advective mass transport (calculated as the lowest order approximation to the Lagrangian residual velocity) is approximately twice that of the Eulerian residual velocity and in the same direction in the deep channel. The Stokes drift velocity contribution to the Lagrangian residual velocity enhances the upriver Eulerian residual velocity transport on the north side of the transect and only slightly increases the downriver transport on the south side.

I. Introduction

The James River is the southernmost major tributary of Chesapeake Bay. Approximately one-third of its length, the 160 km segment seaward of Richmond, is tidal and about one-third of this is estuarine. The central half of the estuarine portion contains some of the most productive seed oyster beds in the Chesapeake Bay system. Oysters spawn in the James River in summer and early fall. Their larvae stay suspended in the water column and drift with currents for about 10 to 20 days before settling to the bottom. Successful recruitment requires, among other things, a large number of larvae over a favorable hard substrate (e.g., oyster beds) at the time in their development when they must attach for permanent residence. The paths of water mass movement from the spawning stock to ultimate settling is thus crucial. In fact, a pioneering work on estuarine circulation was conducted in the James River (Pritchard, 1952) for the purpose of understanding the oyster recruitment processes. That investigation led to the classical two-layered estuarine circulation model in which the Eulerian residual velocity direction is downriver in a less saline upper layer and upriver in a saltier bottom layer. As a result of that study, Pritchard (1953) suggested that the upriver residual current in the bottom layer served as a mechanism for transport of oyster larvae from the beds of market oysters, near the mouth of the river, up into the seed bed regions. It was also pointed out by Pritchard (1952) that the non-tidal circulation exhibited a lateral variation across the river. There is a tendency for the downriver flow in the upper layer to crowd towards the southwest side of the river, and for the upriver flow in the lower layer to crowd towards the northeast side of the river. This results in the boundary between the two layers being deeper towards the southwest side, and shallower towards the northeast side of the river.

Since the 1960's, there has been a trend of decreasing oyster production both within the Commonwealth of Virginia and within the Chesapeake Bay system. This

Coastal and Estuarine Studies, Vol. 38
R.T. Cheng (Ed.)
Residual Currents and Long-term Transport

study represents one component of a multi-disciplinary study by the Commonwealth to improve the economics of the oyster industry. The objective of this study was to delineate the transport pathways of oyster larvae from their spawning to settling. In order to attain this objective, a series of field measurements were conducted from 1984 to 1987. This paper describes the residual transport processes through a transect located near the downriver limit of the seed oyster beds.

II. Field Measurements and Data Analyses

Almost all of the active oyster beds in the James River are located in shallow waters upriver of the James River Bridge (Figure 1). After spawning, the oyster

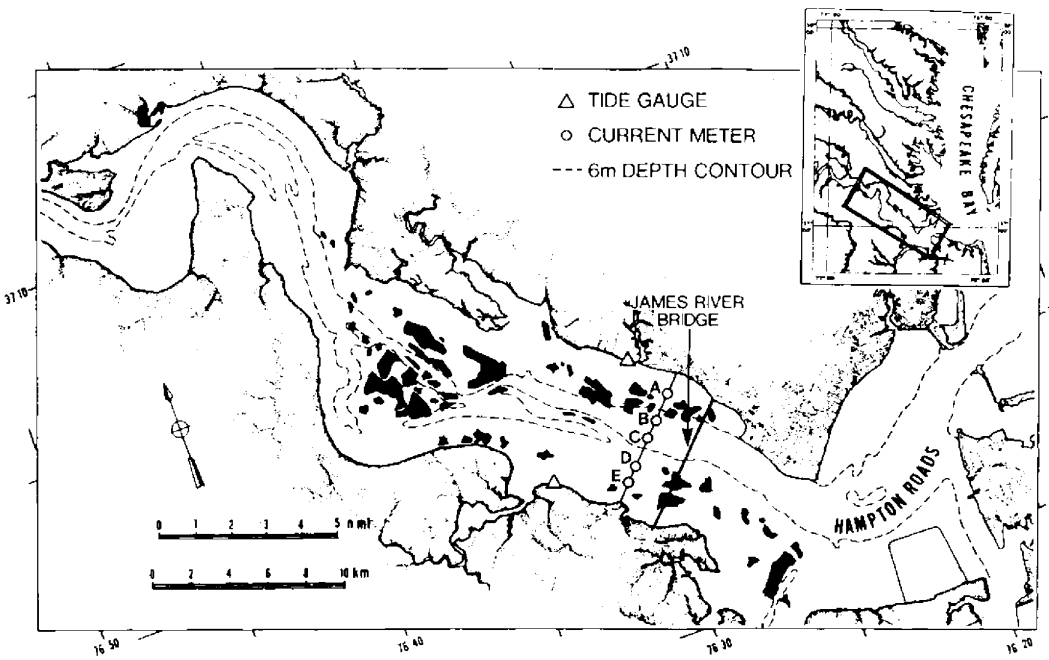

FIGURE 1. The James River Estuary, with tide gauge and current meter stations. Seed oyster beds are shown as irregularly shaped darkened areas.

are suspended in the surface layer of waters that have a net or residual velocity in the downriver direction. To have successful recruitment, there must be net upriver transport pathways at the downriver limit of the oyster beds, otherwise the oyster larvae would be flushed out of the river and be lost from the system. To study the net transport patterns on the downriver side of oyster beds, a total of 14 current meters were moored at 5 stations spanning the river near the James River Bridge. The station locations and the depths of meters at each station are indicated, respectively, in Figs. 1 and 2. The current meter station in the channel was maintained from June to November 1985, and the others for the month of July only. Eight of the current meters were equipped with conductivity and temperature sensors. Average velocity magnitude and direction, and conductivity and temperature if available, were recorded in the meters at half hour intervals. One of the meters at station A failed to provide any data. The meter at the southwest side of the transect provided only 10 days of data.

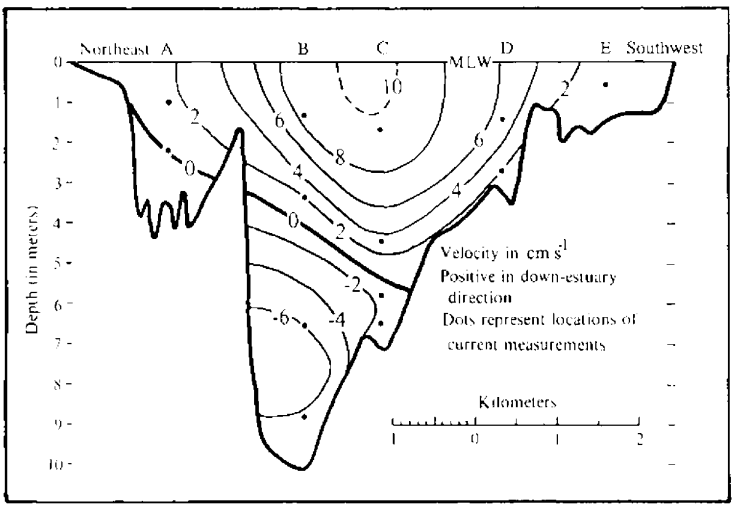

FIGURE 2. Distribution of mean Eulerian residual velocity in a transect across the estuary.

Concurrent with the current meter deployment, a tide gauge was installed on each side of the river. Water surface elevation was measured every 6 minutes and recorded on paper tape. Hourly tidal heights were obtained by averaging 5

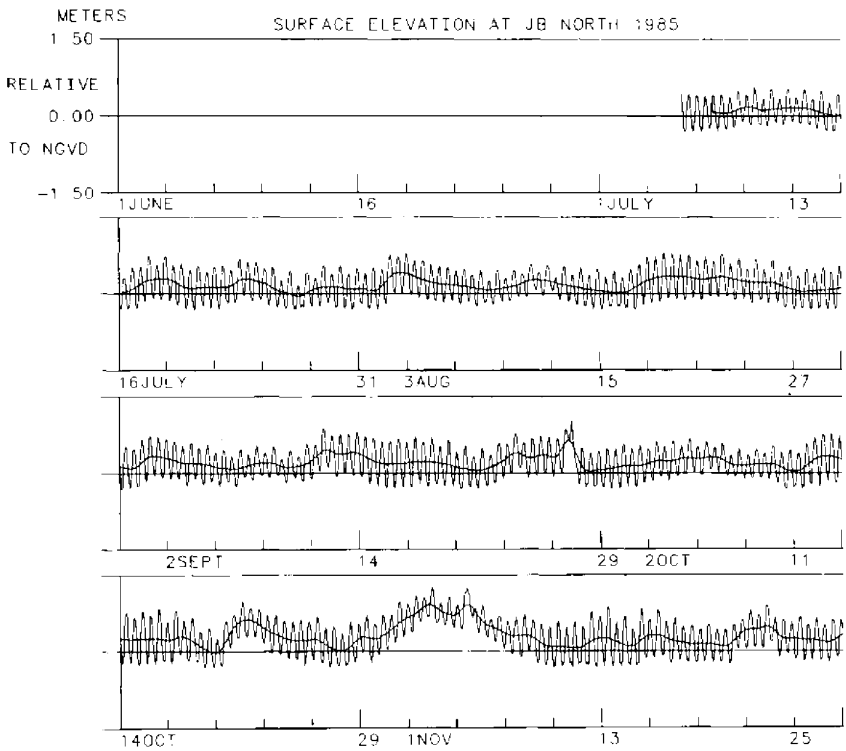

FIGURE 3. Water surface elevation at north side station (both hourly data and low-pass filtered data are shown).

consecutive data points centered on the hour. The hourly data were then adjusted to water surface elevation relative to NGVD (National Geodetic Vertical Datum). The data were then subjected to a low-pass filter to remove the tidal components and other high frequency fluctuations. The filter has a cut-off frequency of (36 hours)$^{-1}$ and filter window of 96 hours. The hourly heights and filtered water surface variations are plotted as functions of time in Figure 3 for the tide gauge station on the north side of the river.

The current data were analyzed to determine the principal axis, or the dominant flow direction, along which the sum of absolute values of velocity components from all data points was maximum. This axis can be determined for each meter location as follows:

$$P = 0.5 \tan^{-1} \frac{2\overline{uv}}{\overline{v^2} - \overline{u^2}} \qquad (1)$$

where P is the angle of principal axis relative to true north, u and v are, respectively, the east and north components of the velocity, and overbars indicate averaging over all data points.

To allow for the possibility that the directions of flood and ebb flows might not be diametrically opposed, the data points were split into two groups by a line perpendicular to the direction with angle P. An angle, E or F, was determined separately for each group of data. The resulting two directions represent the ebb and flood directions, respectively, at the current meter location. The procedure to determine E and F may be repeated by regrouping data points. Those data lying within 90° on either side of direction with angle E (or F) were considered as ebb (or flood) current. The new angles E and F were then determined for each of the new groups of data. It was found that the procedure converged very rapidly, and the second adjustment usually resulted in insignificant refinement.

The most apparent feature of the currents is their strong directionality along principal axes of flood and ebb flows, as illustrated by a polar plot in Figure 4. Table 1 lists the angles P, E and F for each current meter, showing that except

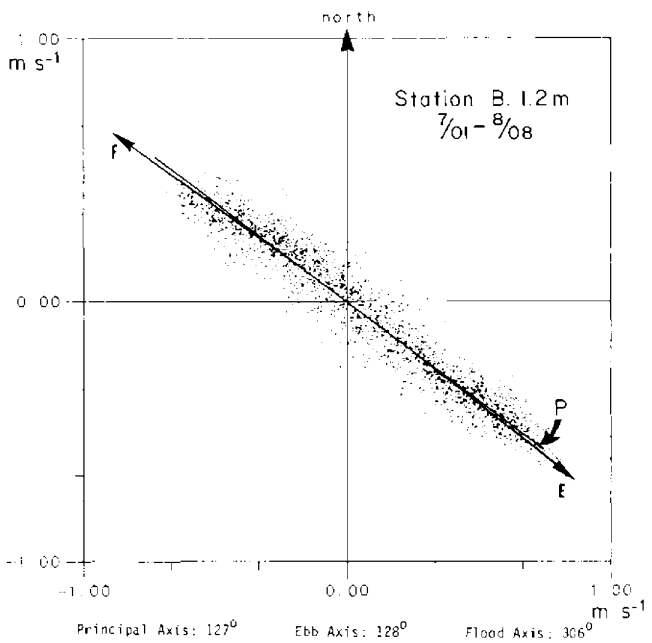

FIGURE 4. Sample of polar plot of current meter data.

station C, the flood and ebb flows were approximately opposite to each other. The principal axes of the surface currents were generally parallel to the shoreline, while data from station B, the station in the channel, show that the principal axes rotated progressively to a direction parallel to the bathymetric contours near the bottom. For the purpose of calculating mass transport, a longitudinal axis was chosen in a direction perpendicular to the transect in which the current meters were deployed. The data were resolved about this direction to produce the longitudinal and transverse components of the velocity series before further analyses were performed.

Table 1. Mean velocity components and principal directions for the July 2 to 31, 1985 data (positive u direction is ebb along the principal axis; the direction angles P, E and F are relative to true north).

Station	Depth m	P	E degree	F	u cm/s	v cm/s
A	0.7	128	130	305	1.1	-1.7
	1.9	126	128	304	-0.04	-0.99
B	1.2	127	128	306	8.9	-1.9
	3.1	120	120	300	1.8	0.28
	6.3	105	106	284	-6.6	-2.5
	8.5	101	108	279	-6.6	-3.8
C	1.5	112	105	307	11.0	8.4
	4.3	115	119	289	3.0	-2.8
	5.6	109	99	301	-0.74	4.8
	6.6	112	105	299	-0.88	2.2
D	1.2	110	113	285	5.4	-1.4
	2.4	110	114	286	1.7	-1.5
E	0.2	125	130	302	0.15	-1.4

III. Eulerian Residual Velocity

Mean Eulerian residual velocities were obtained by averaging the longitudinal and transverse components, respectively, for each current meter over a 29-day period. The cross-sectional distribution of the longitudinal component is presented as isotachs in Figure 2. The distribution shows the characteristic partially mixed estuary circulation pattern in the northeastern half of the transect with the mean current directed downriver in the upper layer and upriver in the lower layer. The level of no net motion tilts downward to the southwest, such that the net flow was directed downriver at all depths on the southwestern half of the transect. The upriver flow existed only in the deeper portion of the transect and near the bottom of the shallow waters along the north shore. This pattern of flow distribution was reported by Pritchard (1952), and may be explained in terms of topographic and geostrophic effects on both the tide induced and density driven portions of the residual circulation (Hamrick, 1986, 1988).

The string of current meters at the station in the channel was maintained for six months, allowing mean longitudinal velocity components to be calculated for several periods representing different hydrological conditions. The results are presented in Figure 5 to demonstrate the vertical distribution of Eulerian residual velocity for each period. It is seen that all velocity distributions possess a distinct feature of two-layered circulation. These data represent freshwater discharges ranging from as low as 35% of annual mean discharge in July to as high as 1200% in early November. A curve representing the velocity profile under low river flow conditions is also presented in Figure 5. This curve was drawn based on the data from three periods, June 1 to July 1, July 2 to August 19, and September 12 to November 3, each having an average river discharge of less than half of the mean

annual discharge. The other sets of data may be considered as transient deviations from this typical velocity profile. The high river flow from August 19 to 26, representing 325% of the annual mean discharge, affected only the velocity in the upper layer. A flood flow condition (November 3 to 10) was necessary to noticeably suppress the upriver flow in the lower layer. The post flood period (November 10 to 27) showed a significant increase in upriver flow, which helped to increase salinity depressed by the preceeding flood discharge.

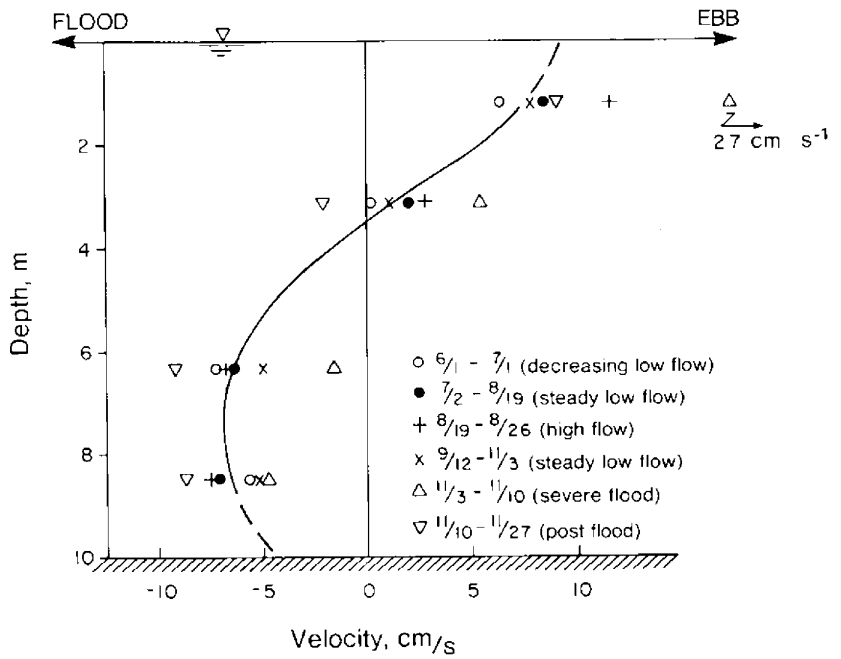

FIGURE 5. Vertical distribution of mean Eulerian residual velocity at the station in the main channel (the curve represents velocity profile in low river flow conditions).

To investigate the temporal variability of the Eulerian residual velocities, the longitudinal components of the half-hourly velocity data for the channel station were subjected to a low-pass filter with a cut-off frequency of (36 hours)$^{-1}$. The filtering process essentially eliminates the diurnal and semi-diurnal tidal constituents, and velocity fluctuations of higher frequencies. The resulting filtered series were considered to be the Eulerian residual velocity, and Figure 6 shows the residual velocities at Station B. The figure shows that the residual currents were directed downriver near the surface and upriver near the bottom, except for several brief periods each lasting less than 3 days. The deviation from the characteristic two-layered circulation usually took the form of upriver flow at all depths for about 2 days followed by strong downriver flow in the upper layer or at all depths. The period from 20 to 23 October typified these periods of deviation from normal condition. Excluding the time when surface or bottom current data were not available, the characteristic two-layered circulation prevailed for 90% of the time. Of the 10% of the time during which other circulation patterns prevailed, half of them were the result of Hurricane Juan, which passed by the area in late October and its induced flooding in early November. This is in contrast with observations reported for the Potomac River (Elliot, 1978) and Chesapeake Bay (Pritchard and Vieira, 1984), which indicated that the characteristic two-layered circulation of the partially mixed estuary was frequently disrupted by meteorological forcings. Elliot (1978) calculated that the characteristic circulation occurred about 43% of the time at a station in the Potomac River.

Though the pattern of the two-layered circulation in the James River estuary was highly persistent, the strength of circulation was quite variable, mainly influenced by the meteorological forcings. No apparent response to spring-neap fortnightly variation was observed. This is consistent with the numerical model results (Cerco and Kuo, 1983) which indicate that depth average salinity did not vary with the spring-neap cycling; and since the longitudinal salinity gradient is the primary driving force of the two-layered circulation, little variability would be expected.

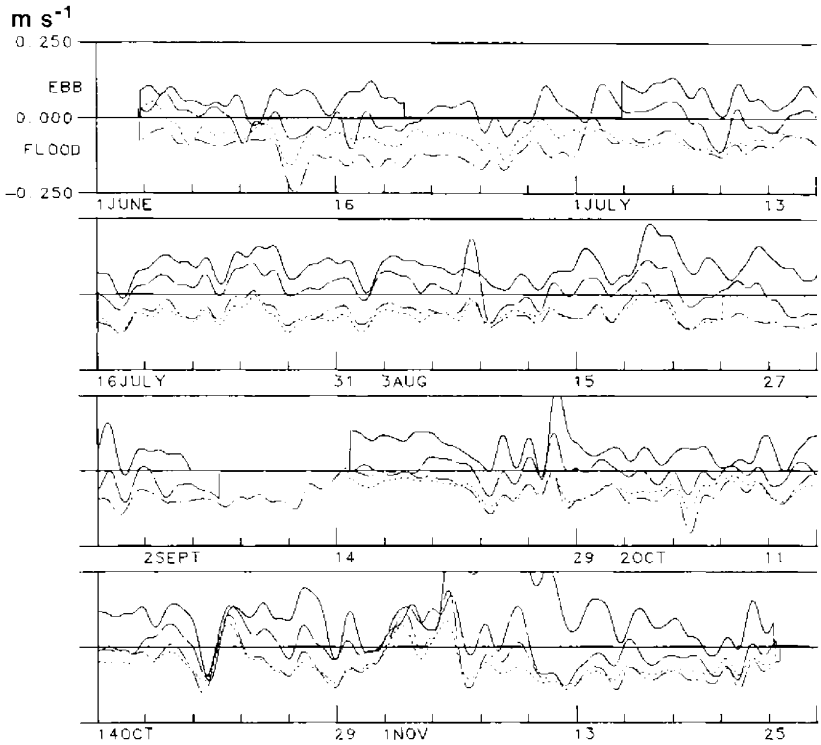

FIGURE 6. Temporal variation of Eulerian residual velocities at station B (— 1.2 m depth, — — 3.1 m depth, —•— 6.3 m depth, ------ 8.5 m depth).

The mean Eulerian velocity distribution presented in Figure 2 was used to calculate the apparent residual transport through the transect. The downriver and upriver transports were calculated separately by integrating the longitudinal Eulerian residual velocity over the cross-sectional area above and below the level of no net motion respectively. To calculate the downriver transport, the velocity was integrated up to mean water level assuming no variation above mean low water. The calculation resulted in apparent residual transports of 1150 and 306 m^3/s, respectively, for the downriver and upriver flows. The fresh water discharge into the river was fairly steady during the period of current meter deployment over the whole transect, having an average value of 80 m^3/s, which is much lower than the difference between the net downriver and upriver flows. Therefore, to maintain mass balance, the cross sectional integral of the longitudinal Stokes drift velocity must contribute about 764 m^3/s to the upriver flow, which was more than twice of that contributed by Eulerian residual velocity. These results suggested that additional analyses accounting for the relationship between the Eulerian residual velocity, the Stokes drift velocity and the Lagrangian residual velocity or residual mass transport velocity be performed.

IV. Residual Mass Transport Velocity

It is now generally accepted that the Lagrangian residual velocity field is the appropriate representation of long-term advective mass transport in long wave dominated estuarine flows. For a vertically uniform distribution of the horizontal velocity components, Longuet-Higgins (1969) showed the two-dimensional lowest order approximation to the Lagrangian residual velocity, termed the residual mass transport velocity, to be the sum of the Eulerian residual velocity and the Stokes drift. Feng et al. (1986a, b) extended this work to second order by adding an additional term called the Lagrangian drift. Hamrick (1987) derived long-term mass transport equations for weak and strong vertical stratification in a vertically stretched and horizontal curvilinear coordinate system. For the weak stratification case, the long-term advective mass transport velocity was shown to be the curvilinear coordinate system generalization of the vertically uniform, two-dimensional horizontal residual mass transport velocity derived by Longuet-Higgins (1969). For the strong stratification case, the long-term advective mass transport velocity was shown to be a three-dimensional generalization of the two-dimensional residual mass transport velocity.

In a vertically stretched, $0 \le z \le 1$, horizontal Cartesian coordinate system, the three-dimensional residual mass transport velocity, or first order approximation to the Lagrangian residual velocity, (u_L, v_L, w_L), is

$$u_L = \langle u_1 \rangle + \frac{\langle h_1 u_0 \rangle}{h_0} + \frac{1}{h_0}\frac{\partial}{\partial y}(h_0 B_z) - \frac{1}{h_0}\frac{\partial}{\partial z} B_y \tag{2}$$

$$v_L = \langle v_1 \rangle + \frac{\langle h_1 v_0 \rangle}{h_0} + \frac{1}{h_0}\frac{\partial}{\partial z} B_x - \frac{1}{h_0}\frac{\partial}{\partial x}(h_0 B_z) \tag{3}$$

$$w_L = \langle w_1 \rangle + 0 + \frac{\partial}{\partial x} B_y - \frac{\partial}{\partial y} B_x \tag{4}$$

$$B_x = \langle v_0 \int w_0 dt_0 \rangle \tag{5}$$

$$B_y = \langle w_0 \int u_0 dt_0 \rangle \tag{6}$$

$$B_z = \langle u_0 \int v_0 dt_0 \rangle \tag{7}$$

with the continuity equations

$$\frac{\partial}{\partial x}(h_0 u_L) + \frac{\partial}{\partial y}(h_0 v_L) + \frac{\partial}{\partial z} w_L = 0 \tag{8}$$

$$\frac{\partial}{\partial x}(h_0 \langle u_1 \rangle + \langle h_1 u_0 \rangle) + \frac{\partial}{\partial y}(h_0 \langle v_1 \rangle + \langle h_1 v_0 \rangle) + \frac{\partial}{\partial z}\langle w_1 \rangle = 0 \tag{9}$$

also presented for completeness. The operator, $\langle\ \rangle$, denotes a low pass filter, while the numerical subscripts indicate ordering in the barotropic long wave Froude number used as the perturbation parameter in deriving Eqs.(2-4). The Eulerian residual velocity, $\langle u_1, v_1, w_1 \rangle$, is formally and operationally equivalent to $\langle u, v, w \rangle$, the low pass filter of the instantaneous or discretely sampled Eulerian velocity, while h_0 is the equivalent of $\langle h \rangle$, the low pass filter of the total water column depth h. The long wave or tidal components of the velocity field are (u_0, v_0, w_0) and are equivalent to $(u,v,w) - \langle u,v,w \rangle$, the high pass filter of the Eulerian velocity, while h_1, tidal surface elevation fluctuation is equivalent to $h - \langle h \rangle$, the high pass filter of the total water depth.

The last three terms on the right in Eqs.(2-4), respectively, represent the Stokes drift velocity, and the first of these terms, of the form $\langle h_1 u_0 \rangle / h_0$, may be

referred to as the wave transport velocity portion of the Stokes drift. The remaining terms involving the variables (B_x, B_y, B_z) may be referred to as the vector potential transport velocity portion of the Stokes drift velocity, since Eqs.(2-4) are the scalar components of

$$\mathbf{q}_L = \mathbf{q}_{ET} + \nabla \times \mathbf{B} \tag{10}$$

in a stretched vertical coordinate system. The sum of the Eulerian residual velocity and the wave transport velocity, $\mathbf{q}_{ET}$, is often termed the Eulerian residual transport velocity which satisfies the Eulerian continuity equation, Eq.(9). It also may be shown that Eq.(10) is equivalent to

$$\mathbf{q}_L = \langle \mathbf{q}_1 \rangle + \langle \int \mathbf{q}_0 dt \cdot \nabla \, \mathbf{q}_0 \rangle \tag{11}$$

the original form presented by Longuet-Higgins (1969). Referral is made to Hamrick (1987, 1989) for derivations and further discussion of the results represented by Eqs.(2-10).

The expressions for the residual mass transport velocity, Eqs.(2-4), derived in a stretched vertical coordinate system, can be applied to the analysis and interpretation of velocity measurements at fixed vertical locations with relative errors not exceeding the ratio of tidal surface displacement amplitude to mean or low pass total depth. For the transect of the James River under consideration, this ratio, which is also an estimate of the barotropic long wave Froude number, has an average value of 0.08. For measurements of horizontal velocity components, (u,v), over the cross sectional transect, now defined as the plane x = 0, it is possible to estimate the first three of the four terms on the right of Eq.(2), contributing to the longitudinal residual mass transport velocity, u_L. Only the first two terms on the right of Eq.(3), contributing to the transverse residual mass transport velocity, v_L, can be estimated, while of course none of the terms in Eq.(4) can be estimated since the vertical velocity w cannot be determined from horizontal velocity measurements in a plane.

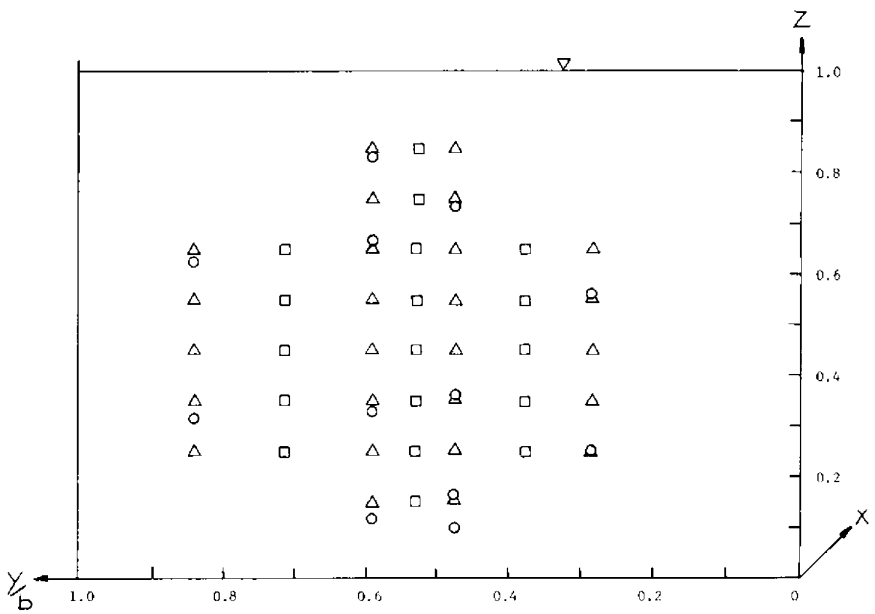

FIGURE 7. Location of points in stretched transect cross section used to compute the residual mass transport velocity. 12 current meter locations, o, 26 interpolation points, Δ, 18 residual mass transport velocity points, □ .

The procedure used in estimating the first three terms on the right of Eq.(2) and the first two terms on the right of Eq.(3), first involved extraction of synchronous 512 hour time series of horizontal velocity components for twelve of the current meters and of the water surface elevation for the two tide gauges. Using known depths at the current meter locations and interpolating across the transect between the two tide gauges, time series of total depth at the current meter locations were generated. The horizontal velocity time series, with u being longitudinal, normal to the transect and v being transverse, tangent to the transect, and the total depth time series were filtered to produce the high pass time series, u_0, v_0 and h_1 and the low pass time series $\langle u_1 \rangle$, $\langle v_1 \rangle$ and h_0.

The filtered velocity time series at the twelve current meter locations were used to generate filtered velocity time series at 26 new, uniform in the vertical, locations using linear interpolation as shown in Figure 7. Filtered time series of the horizontal components of the wave transport velocity, $\langle h_1 u_0 \rangle / h_0$ and $\langle h_1 v_0 \rangle / h_0$, and the vertical component of the vector potential, B_z, defined by Eq.(7), were calculated at these locations. Time series of the longitudinal components of the Eulerian residual velocity, the wave transport velocity and the transverse, y, gradients of the vector potential component B_z, corresponding to the first three terms on the right of Eq.(2) were then calculated at 18 new locations, as shown in Figure 7, using linear interpolation and finite difference differentiation. To eliminate filter contaminant at the ends of these series, as well as to determine mean values for presentation and interpretation, the mean values of the interior one half series length were determined.

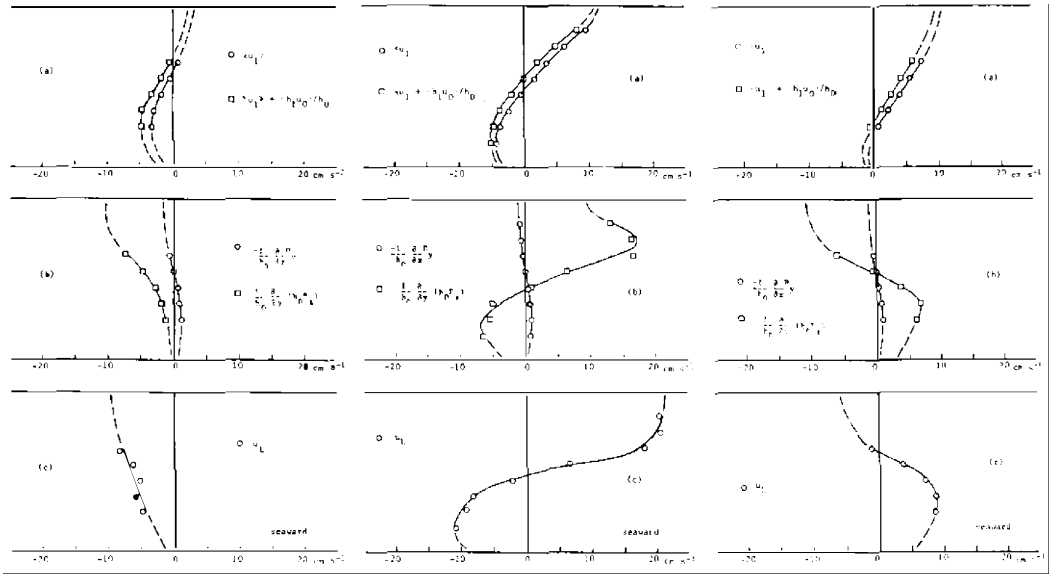

a) northeast b) central channel c) southwest

FIGURE 8. Vertical distribution of the Eulerian residual, Stokes drift and residual mass transport velocity, toward the northeast shore (a), the central channel (b), and toward the southwest shore (c). [Eqs.(7) and (15) were used to calculated B_z and B_y respectively].

The final results of the analysis procedure are mean values of the longitudinal components of the Eulerian residual velocity, $\langle u_1 \rangle$, the wave transport velocity, $\langle h_1 u_0 \rangle / h_0$, and the transverse gradient portion, $\partial(h_0 B_z)/h_0 \partial y$, of the vector potential transport velocity at 18 locations in the cross sectional transect. The results are presented in Figure 8a, b, c, which respectively represent vertical profiles based on points 1-5, toward the northeastern shore, (8a), points 6-13, in the central region near the channel, (8b), and points 14-18 toward the southwestern shore, (8c).

The top panels of Figure 8 show the vertical distribution of the Eulerian residual velocity, $\langle u_1 \rangle$, and the Eulerian residual transport velocity, $\langle u_1 \rangle + \langle h_1 u_0 / h_0 \rangle$, composed of the sum of the Eulerian residual velocity and the wave transport velocity. In the central portion of the transect, both the Eulerian residual velocity and the Eulerian residual transport velocity exhibit the classical circulation pattern of seaward flow in the surface layer and landward flow in the bottom layer, with the level of zero transport velocity being near mid-depth. The difference between the two profiles, the wave transport velocity, is nearly uniform over the depth, with a value of 1.2 cm/s, and directed landward consistent with the direction of wave propagation. In the northeastern portion of the transect, both the Eulerian residual and the Eulerian residual transport velocity exhibit the classical circulation pattern. However, the landward transport in the bottom layer is dominant with the level of zero transport velocity being approximately two-thirds of the depth up from the bottom. The wave transport velocity is again nearly uniform over the depth, and directed landward with magnitude of 1.7 cm/s, which is approximately 40% greater than that in the central region. In the southwestern portion of the transect, both the Eulerian residual and the Eulerian residual transport velocity again exhibit the classical circulation pattern. However, the seaward transport in the surface layer is dominant with the level of zero transport velocity being approximately three-fourths of the depth down from the surface. The wave transport velocity is nearly uniform over the depth and directed landward with a magnitude of 1.2 cm/s.

The middle panels of Figure 8 show the vertical distribution of the transverse gradient portion, $\partial(h_0 B_z)/h_0 \partial y$, of the vector potential transport velocity. In the northeastern region of the transect this portion of the vector potential transport velocity is entirely landward. In the central region, there is a two layer distribution with a predominance of seaward transport in the surface layer. The southwest region shows a two layer distribution, however, the transport in the surface layer is landward.

As previously noted, the vertical gradient portion, $-\partial B_y/h_0 \partial z$, of the vector potential transport velocity cannot be directly determined since B_y, defined by Eq.(6), involves the vertical velocity that cannot be determined from measurements of horizontal velocity in a planar transect. However, the uniformity of the wave transport velocity over the depth suggests that there is little phase variation in the longitudinal high pass velocity, u_0, thus allowing the vertical distribution of u_0 to be approximated by

$$u_0 = \bar{u}_0[1 + f(z)] \tag{12}$$

where $\bar{u}_0$, is the average of u_0 over the vertically stretched coordinate, $0 \leq z \leq 1$. A similar expression for the transverse high pass velocity may be assumed. The order zero continuity equation relating high pass depth and velocity is

$$\frac{\partial}{\partial t_0} h_1 + \frac{\partial}{\partial x}(h_0 u_0) + \frac{\partial}{\partial y}(h_0 v_0) + \frac{\partial}{\partial z} w_0 = 0 \tag{13}$$

(Hamrick, 1987, 1988). Inserting Eq.(12) and a similar expression for v_0 into Eq.(13) and making use of the depth average of Eq.(13) gives

$$\frac{\partial}{\partial z} w_0 = f(z) \frac{\partial h_1}{\partial t_0} , \tag{14}$$

allowing Eq.(6) to be evaluated as

$$B_y = - \langle h_1 \bar{u}_0 \rangle (1 + f(z)) \int_0^z f(z) dz . \tag{15}$$

Since $\langle h_1 \tilde{u}_0 \rangle$ is the depth integral of the wave transport velocity and can be readily calculated, approximate estimation of B_y and the vertical gradient portion, $-\partial(B_y)/h_0\partial z$, of the vector potential transport velocity is readily accomplished upon choosing a suitable distribution function, f(z). The middle panels in Figure 8 show the vertical distributions obtained using f(z) corresponding to a parabolic velocity profile. The distribution is two-layered with landward transport in the surface layer and the magnitude is substantially less than that of the transverse gradient portion of the vector potential transport velocity.

The vertical distributions of the longitudinal residual mass transport velocity, the lowest order approximation of the longitudinal Lagrangian residual velocity, are shown in the bottom panels of Figure 8. In the northeastern region of the transect, the residual mass transport velocity is landward over the entire depth resulting from the addition of an entirely landward Stokes drift velocity to the classical two-layered Eulerian residual velocity. In the central region of the transect, the residual mass transport velocity has a classical two-layered distribution, with a dominance of seaward transport in the surface layer, resulting from the two-layered distribution of the Stokes drift velocity reinforcing the classical two-layered distribution of the Eulerian residual velocity. In the southwestern region of the transect, the residual mass transport velocity has a reverse two-layered distribution with a dominance of seaward transport in the bottom layer.

V. Discussion and Conclusion

The results of the preceeding section have shown that the distribution of the residual mass transport velocity, or lowest order approximation to the Lagrangian residual velocity, differs considerably from the distribution of the Eulerian residual velocity and the Eulerian residual transport velocity over a transect normal to the longitudinal axis of the James River. For this particular transect, the persistent longitudinal Eulerian residual velocity distribution is significantly influenced by topographic and geostrophic effects, with landward flow favoring the region toward the northeastern shore. The addition of the Stokes drift, and in particular the transverse gradient portion of the vector potential transport velocity, to the Eulerian residual velocity served primarily to intensify the large scale horizontal circulation feature of landward transport along the northeastern shore region and seaward transport along the southwestern shore region, while also greatly intensifying the two-layered transport structure in the central channel region. These general features of the residual mass transport velocity distribution are consistent with hypothesized transport pathways of oyster larvae in the lower James River.

The results of this study are significant in pointing to the necessity of computing the residual mass transport velocity, as well as the Eulerian residual velocity, as part of current meter data analyses. The inability of completely determining the three dimensional structure of the horizontal components of the residual mass transport velocity from horizontal current measurements in a planar transect suggests the need for alternate current meter moorings. One possibility would be to deploy horizontal velocity measuring current meters over two planar transects, on the order of a tidal excursion apart, normal to the longitudinal axis of an estuary channel. Tide gauges would be located near both shores intermediate between the transects. This arrangement would allow complete determination of both horizontal residual mass transport velocity components over the intermediate transect.

In conclusion, this study has shown that field current measurements and their subsequent Eulerian and Lagrangian residual analyses can be used to better understand the transport of materials in an estuary system. In particular, the Eulerian residual current field was shown to be persistent during a time interval critical for oyster spawning and the residual mass transport velocity field, although considerably different from the Eulerian residual velocity field, exhibited an overall pattern favorable to oyster larvae transport. Since the hydrographic conditions in the James River are fairly steady during summer months, it is reasonable to expect that the characteristics of the residual mass transport velocity field calculated from one month of data should be representative.

This paper is contribution number 1553 from the Virginia Institute of Marine Science, College of William and Mary, Gloucester Point, Virginia.

VI. References

Cerco. C. F. and A. Y. Kuo, 1983: Two-dimensional transient behavior of estuarine salinity. Proceedings, Conference on Frontiers in Hydraulic Engineering, ASCE/MIT, Cambridge, Mass. 375-379.

Elliott, A. J., 1978: Observations of the meteorological induced circulation in the Potomac Estuary. Estuarine and Coastal Marine Science, **6**, 285-299.

Feng, S., R. T. Cheng, and P. Xi, 1986a: On tide-induced residual current and residual transport, Part 1, Lagrangian Residual Current. Water Resources Research, **22**(12), 1623-1634.

Feng, S., R. T. Cheng, and P. Xi, 1986b: On tide-induced residual current and residual transport, Part 2, Residual Transport with Application in South San Francisco Bay, California. Water Resources Research, **22**(12), 1635-1646.

Hamrick, J. M., 1986: Subtidal circulation and transport in estuaries. In Advancements in Aerodynamics, Fluid Mechanics and Hydraulics. ASCE.

Hamrick, J. M., 1987: Time averaged estuarine mass transport equations. Proceedings, National Conference on Hydraulic Engineering, ASCE, Williamsburg, VA 624-629.

Hamrick, J. M., 1989: The dynamics of long-term advective transport in estuaries. This volume.

Longuet-Higgins, M.S., 1969: On the transport of mass by time-varying ocean currents. Deep Sea Research, **16**, 431-447.

Pritchard, D. W., 1952: Salinity distribution and circulation in the Chesapeake Bay estuarine system. J. of Marine Research, 1(2), 106-123.

Pritchard, D. W., 1953: Distribution of oyster larvae in relation to hydrographic condition. Proceedings, Gulf and Caribbean Fisheries Institute, 5th annual session. 123-132.

Pritchard, D. W. and M. E. C. Vieira, 1984: Vertical variations in the residual current response to meteorological forcing in the mid-Chesapeake Bay. In The Estuary as a Filter, V. S. Kennedy (ed.), Academic Press, Inc., Orlando, Florida.